

# A Critical Examination of Hypernova Remnant Candidates in M101. I. MF 83

Shih-Ping Lai, You-Hua Chu<sup>1</sup>, C.-H. Rosie Chen<sup>1</sup>

*Astronomy Department, University of Illinois, 1002 W. Green Street, Urbana, IL 61801;  
slai@astro.uiuc.edu, chu@astro.uiuc.edu, c-chen@astro.uiuc.edu*

Robin Ciardullo<sup>1</sup>

*Department of Astronomy and Astrophysics, Pennsylvania State University, 525 Davey  
Laboratory, University Park, PA 16802; rbc@astro.psu.edu*

and

Eva K. Grebel<sup>2,3</sup>

*Department of Astronomy, University of Washington, Seattle, WA 98195-1580  
and  
Max-Planck-Institut für Astronomie, Königstuhl 17, D-69117 Heidelberg, Germany;  
grebel@mpia-hd.mpg.de*

## ABSTRACT

The SNR candidate MF 83 in M101 is coincident with a very luminous X-ray source. Based on the high X-ray luminosity, it has been suggested that MF 83 is a “hypernova remnant” requiring an explosion energy about two orders of magnitude higher than normal supernovae. We have analyzed high-quality ground-based and *HST* observations of MF 83, and find that MF 83 is a star formation region, consisting of a large ionized gas shell and four H II regions along its periphery. Continuum images show OB associations in these H II regions and within the large shell. The shell has an expansion velocity of  $\sim 50 \text{ km s}^{-1}$  and a diameter of  $\sim 270 \text{ pc}$ . The optical properties of this shell in MF 83 are

---

<sup>1</sup>Visiting astronomer, Kitt Peak National Observatory, National Optical Astronomy Observatories, operated by the Association of Universities for Research in Astronomy, Inc., under a cooperative agreement with the National Science Foundation.

<sup>2</sup>Visiting astronomer, Michigan-Dartmouth-MIT Observatory.

<sup>3</sup>Hubble Fellow.

similar to those of X-ray-bright superbubbles in the Large Magellanic Cloud. If the X-ray emission is indeed diffuse, the implied thermal energy in MF 83 is high, a few  $\times 10^{52}$  ergs. This amount of thermal energy requires a large number of concentrated supernova explosions or one powerful explosion. Future X-ray observations with a high angular resolution are needed to resolve the diffuse emission and point sources in MF 83, in order to determine more accurately the thermal energy in the shell interior and its required explosion energy.

*Subject headings:* galaxies: individual (M101) – supernova remnants – X-rays: ISM – ISM: bubbles – ISM: H II regions – ISM: kinematics and dynamics

## 1. Introduction

It has been generally accepted that a supernova’s explosion energy carried by its ejecta to form a supernova remnant (SNR) is roughly  $10^{51}$  ergs (Jones et al. 1998). Upon analyzing the X-ray emission from SNRs in the giant spiral galaxy M101, Wang (1999) discovered two SNRs that appeared to require explosion energies one to two orders of magnitude higher. One of these SNRs, NGC 5471B, is inside the giant H II region NGC 5471 (Skillman 1985; Chu & Kennicutt 1986). The other SNR, MF 83 (notation from Matonick & Fesen 1997), also appears to be associated with a star formation region (Chu, Chen, & Lai 2000).

Similarly high energies have been frequently found in gamma-ray bursts (GRBs). As some GRBs have afterglows several hundred times more luminous than the brightest supernovae, they have been dubbed “hypernovae.” Some GRBs have been observed to be near star-forming regions (Paczynski 1998). Because of the similarities in the energy requirement and the interstellar/stellar environment, Wang (1999) called the two super-energetic SNRs in M101 “hypernova remnants,” although the association of hypernova remnants to the GRBs has been recently questioned by Paczynski (2000).

Regardless of the GRB connection, SNRs with such large explosion energies are unusual and therefore warrant further investigation. To study the physical nature of the two hypernova remnants in M101, we have obtained deep images with ground-based telescopes, high-resolution images with the *Hubble Space Telescope*, and high-dispersion spectra with an echelle spectrograph. In this paper (Paper I), we report on the hypernova remnant MF 83. The hypernova remnant NGC 5471B will be presented in Paper II.

The suggestion that MF 83 is super-energetic is based mainly on its high X-ray luminosity (Wang 1999). However, none of the existing X-ray observations have resolved MF 83. It is possible that point sources contribute significantly to MF 83’s X-ray emission, since mas-

sive X-ray binaries are frequently found in star formation regions. Only optical observations can resolve MF 83; therefore, we have used our new observations to examine the physical structure of MF 83 and to seek independent evidence for a powerful explosion. At optical wavelengths, MF 83 is unusually large, with a diameter approaching  $\sim 270$  pc (Matonick & Fesen 1997), if we adopt a distance of 7.2 Mpc for M101 (Stetson et al. 1998). No known SNRs in the Local Group are so large. It is therefore important to measure the expansion velocity of MF 83 in order to assess the validity of its identification as a SNR.

In this paper we report on our investigation of the environment and energetics of the hypernova remnant MF 83 using optical observations. The new observations are described in §2, and the analysis and results are presented in §3. We critically examine the physical properties and nature of MF 83 in §4, and summarize our conclusions in §5.

## 2. Observations

The datasets used in this study include : (1) deep CCD images taken with the Michigan-Dartmouth-MIT (MDM) Hiltner 2.4 m telescope and the Kitt Peak National Observatory (KPNO) Mayall 4 m telescope, (2) high-resolution images taken with the *Hubble Space Telescope* Wide Field/Planetary Camera 2 (*HST* WFPC2), (3) high-dispersion echelle spectra taken with the KPNO Mayall 4 m telescope, and (4) archival *Röntgen Satellite* (*ROSAT*) X-ray images.

### 2.1. Ground-based CCD Images

MF 83 was observed on 1999 April 12 (UT) with the MDM Observatory Hiltner 2.4 m telescope in direct imaging mode. The images were recorded with the thinned, backside-illuminated  $1024 \times 1024$  SITE CCD “Charlotte”. The pixel size was  $24 \mu\text{m}$ . The CCD camera was used at the f/7.5 Cassegrain focus; the field of view was  $4'7 \times 4'7$  and the image scale was  $0''.275 \text{ pixel}^{-1}$ . Images of MF 83 were obtained in the Johnson *B*, *V*, and *I* filters and an  $\text{H}\alpha$  filter ( $\lambda_c = 6563 \text{ \AA}$ ,  $\Delta\lambda = 100 \text{ \AA}$ ). The exposure times in *B*, *V*, *I*, and  $\text{H}\alpha$  were  $1 \times 600$  s,  $3 \times 600$  s,  $2 \times 600$  s, and  $1 \times 900$  s, respectively. Standard IRAF<sup>4</sup> tasks were used to combine multiple exposures and to remove cosmic rays. Cirrus clouds were present during part of the night; therefore, we did not use these images for photometric measurements. The

---

<sup>4</sup>IRAF is distributed by the National Optical Astronomy Observatories, which are operated by the Association of Universities for Research in Astronomy, Inc., under cooperative agreement with the NSF.

seeing was  $1''.7$ ,  $1''.1$ ,  $1''.0$ , and  $1''.3$  in  $B$ ,  $V$ ,  $I$ , and  $H\alpha$ , respectively.

Deep  $H\alpha$  and  $R$ -band images of MF83 are available from a nova search in M101 (Shafter, Ciardullo, & Pritchett 2000), for which multi-epoch  $H\alpha$  and  $R$ -band images were obtained with the KPNO Mayall 4 m telescope in 1994 May, 1995 April, 1996 May, and 1997 March. The  $2048 \times 2048$  T2KB CCD detector was used, yielding a  $16' \times 16'$  field of view and an image scale of  $0''.47 \text{ pixel}^{-1}$ . The  $H\alpha$  filter used was the KPNO1390, which has a central wavelength of  $6567 \text{ \AA}$  and a bandpass of  $74 \text{ \AA}$  FWHM in the converging beam of the telescope. The multi-epoch  $H\alpha$  images were co-added to yield a super-deep  $H\alpha$  image with a net exposure time of 390 min. The  $R$ -band image has an exposure time of 6 min.

A deep  $[\text{O III}]\lambda 5007$  image of MF83 is available from a survey of planetary nebulae in M101 (Feldmeier, Ciardullo, & Jacoby 1997). The  $[\text{O III}]$  image was obtained on 1995 April 5 using the same telescope with the same CCD as the aforementioned deep  $H\alpha$  image. The  $[\text{O III}]$  filter was centered at  $5017 \text{ \AA}$  with a FWHM of  $30 \text{ \AA}$ ; this central wavelength was selected to compensate the redshift of M101. The total exposure time of the  $[\text{O III}]$  image was 120 min. For continuum subtraction, an image was also taken with an off-band green continuum filter centered at  $5312 \text{ \AA}$  with a FWHM of  $267 \text{ \AA}$ . The total exposure time of this green continuum image is 18 min.

Figure 1 shows a cosmic-ray-cleaned MDM  $H\alpha$  image of MF 83 and its environment, and Figure 2 shows MDM images of MF 83 in the  $B$ ,  $V$ ,  $I$ , and  $H\alpha$  bands. The  $H\alpha$  image in Figure 2d has been smoothed with a Gaussian of  $\sigma = 1 \text{ pixel}$  ( $0''.275$ ). Figure 3 presents KPNO 4m images of MF 83 in the  $H\alpha$  and  $[\text{O III}]$ , red and green continua, and continuum-subtracted  $H\alpha$  and  $[\text{O III}]$ . Note that these “ $H\alpha$ ” images are really  $H\alpha + [\text{N II}]$  images, as both MDM and KPNO  $H\alpha$  filters are broad enough to include the  $[\text{N II}]\lambda\lambda 6548, 6583$  lines.

## 2.2. *HST* WFPC2 Images

The *HST* WFPC2 images of MF 83 were obtained on 1999 June 17 for the GO program 6928 – “The Luminous Giant H II Regions in M101.” As MF 83 is only  $\sim 50''$  from the luminous giant H II region NGC 5461, it is serendipitously included in the same Wide Field Camera, WF4 in this case. A Wide Field Camera covers an area of  $79''.7 \times 79''.7$  and has a pixel size of  $0''.0996 \text{ pixel}^{-1}$ . As the observations were designed for NGC 5461, which is much brighter than MF 83, the images are inevitably shallow for MF 83.

The observations were made through the filters  $F547M$  and  $F656N$  (see Biretta et al. 1996 for filter characteristics) for  $2 \times 500 \text{ s}$  and  $2 \times 600 \text{ s}$ , respectively. The  $F547M$  filter is centered at  $5476.3 \text{ \AA}$  with a FWHM of  $483.1 \text{ \AA}$ . This filter isolates an emission-line-free band

similar to, but wider than, the Strömgen  $y$  band. The  $F547M$  images show stars in and near MF 83. The  $F656N$  filter, centered at  $6563.7 \text{ \AA}$  with a FWHM of  $21.4 \text{ \AA}$ , is an  $H\alpha$  filter that does not include the  $[\text{N II}]$  lines. The  $F656N$  images barely detected the  $H\alpha$  emission from MF 83. No useful morphological information can be extracted from these  $F656N$  images.

The calibrated WFPC2 images were produced by the standard *HST* pipeline processes. We processed them further with IRAF and STSDAS routines. The images taken with the same filter were combined to remove cosmic rays and to produce a total exposure map. The combined  $F547M$  image was then corrected for the intensity- and position-dependent charge transfer efficiency by applying a linear ramp with a correction factor chosen according to the average counts of the sky background (Holtzman et al. 1995a). The combined  $F547M$  image was further multiplied by the geometric correction image f1k1552bu.r9h (downloaded from the *HST* archives) to compensate the different effective areas covered by the pixels (Holtzman et al. 1995a; Biretta et al. 1996). This correction is  $\sim 1\text{-}2\%$  near the edges, with a maximum of  $\sim 4\text{-}5\%$  in the corners of the CCD.

The final corrected  $F547M$  image, shown in Figure 4, was used to carry out stellar photometry. We used the APPHOT package in IRAF and followed the procedures for photometry detailed by Whitmore & Heyer (1995). An aperture of 3 pixel radius ( $0''.3$ ) was used to measure the total counts of each stellar source, with the sky brightness determined from a 5-pixel-wide annulus of inner radius 10 pixels. An aperture correction was made to include all the light within the  $0''.5$  standard aperture, as recommended by Holtzman et al. (1995b). The number of counts ( $DN$ ) in each stellar source is converted to an apparent magnitude ( $m$ ) using the formula  $m = -2.5 \times \log_{10}(DN/EXPTIME) + ZEROPOINT$ , where  $EXPTIME$  is the exposure time and  $ZEROPOINT = -2.5 \times \log_{10}(PHOTFLAM) - 21.1$ . The parameter  $PHOTFLAM$  is  $7.747 \times 10^{-18} \text{ ergs s}^{-1} \text{ cm}^{-2} \text{ \AA}^{-1}$  and is a product provided in the image header by the *HST* pipeline processes.

The apparent magnitude in  $F547M$ ,  $m_{F547M}$ , can be converted to the Johnson  $V$  magnitude,  $m_V$ , by applying a correction of  $-0.023 \text{ mag}$  (appropriate for Vega, *HST* Data Handbook), but this correction is negligible compared to the photometric error  $\pm 0.2 \text{ mag}$ . Adopting a distance modulus of  $29.3 \text{ mag}$  ( $= 7.2 \text{ Mpc}$ ) and a visual extinction  $A_V = 1.3 \text{ mag}$  (Matonick & Fesen 1997), we have converted the  $V$  magnitude to absolute visual magnitude  $M_V$ . The right ascension, declination,  $m_{F547M}$ , and  $M_V$  of the sources identified in the  $F547M$  image are listed in Table 2.

### 2.3. KPNO Echelle Spectra

High-dispersion spectra of MF 83 were obtained with the echelle spectrograph on the KPNO Mayall 4 m telescope in two observing runs: 1999 March 2 – 4 and 1999 June 30 – July 2 (UT). The same observing configuration was used in both runs. The 79 line  $\text{mm}^{-1}$  echelle grating 79-63 and the 226 line  $\text{mm}^{-1}$  cross disperser 226-1 were used in conjunction with the long focus red camera to achieve a reciprocal dispersion of  $3.5 \text{ \AA mm}^{-1}$  at the  $\text{H}\alpha$  line. The spectra were imaged with the  $2048 \times 2048$  T2KB CCD detector. The  $24 \mu\text{m}$  pixel size corresponds to  $0''.24 \text{ pixel}^{-1}$  along the slit and  $\sim 3.7 \text{ km s}^{-1} \text{ pixel}^{-1}$  along the dispersion axis. Each echellogram covers at least  $4,300 - 7,000 \text{ \AA}$ , which includes bright nebular emission lines such as  $\text{H}\alpha$ ,  $\text{H}\beta$ ,  $[\text{O III}]\lambda\lambda 4959, 5007$ ,  $[\text{O I}]\lambda 6300$ ,  $[\text{N II}]\lambda\lambda 6548, 6583$ , and  $[\text{S II}]\lambda\lambda 6716, 6731$ .

The journal of observations of MF 83 is given in Table 1. Two orthogonal slit positions, E-W and N-S through the center of MF 83, were observed. Different slit widths were used, resulting in different instrumental widths. The instrumental FWHM, determined by Gaussian fits to the unresolved sky lines (telluric OH lines), is also given in Table 1.

IRAF software was used for data reduction and analysis. The reduction processes included bias subtraction, cosmic ray removal, and quartz flat-fielding to remove the pixel-to-pixel gain variation. As we were mainly interested in the velocity profiles and not the surface brightness variation, we did not use a sky flat to flatten the illumination variation along the slit. To remove the sky lines, a sky spectrum extracted from regions outside MF 83 is scaled and subtracted from the nebular spectrum. In order to improve the S/N ratio, the final spectra of MF 83 were Hanning smoothed over five adjacent pixels (i.e., weighted average with weights of  $1/4, 3/4, 1, 3/4$ , and  $1/4$  for the five pixels). As the data are oversampled, this smoothing does not degrade the spectral resolution.

The spectra of MF 83 obtained in the 1999 March run have low S/N ratios, but they show a line split indicating an overall expansion. The follow-up observations made in the second observing run have longer integration times and show the expansion more clearly. The new spectra will thus be the main echelle data presented in this paper. Figure 5 displays a portion of the N-S echellogram of MF 83 centered on the  $\text{H}\alpha$  and  $[\text{N II}]\lambda 6584$  lines, and a close-up of the sky-subtracted  $\text{H}\alpha$  line.

### 2.4. ROSAT Observations

Both *ROSAT* Position Sensitive Proportional Counter (PSPC) and High Resolution Imager (HRI) observations are available for MF 83 (see Table 2 of Wang, Immler, & Pietsch

1999). These observations are all centered at the nucleus of M101. As MF83 is only  $\sim 4'$  from the nucleus of M101, the point spread function at MF 83 should be similar to that at the center,  $\sim 30''$  for the PSPC and  $\sim 5''$  for the HRI (*ROSAT* Mission Description 1991).

The HRI observations are merged into a 227 ks exposure. The merged HRI image is binned by a factor of two to obtain a pixel size of  $1'' \text{ pixel}^{-1}$ , and smoothed with a Gaussian of  $\sigma = 2$  pixels ( $1''$ ). The smoothed HRI image is presented in Figure 6a, and the X-ray contours are overplotted on the KPNO 4 m  $\text{H}\alpha$  image in Figure 6b.

The PSPC observation has a shorter exposure time, 33.9 ks, and a poorer angular resolution; therefore, the X-ray source at MF 83 is not as well defined in the PSPC observation as in the HRI image. The PSPC data have been integrated over all energy channels (0.1 – 2.4 keV), binned by a factor of 10 to obtain a pixel size of  $5'' \text{ pixel}^{-1}$ , and smoothed with a Gaussian of  $\sigma = 2$  pixels ( $10''$ ). The smoothed PSPC image is shown in Figure 6c, and the X-ray contours are overplotted on the KPNO 4 m  $\text{H}\alpha$  image in Figure 6d.

### 3. Analysis & Results

#### 3.1. Interstellar and Stellar Environment of MF 83

MF 83 is located between two spiral arms of M101 (Figure 1). Having a  $[\text{S II}]/\text{H}\alpha$  ratio of 0.76 and a diameter of  $\sim 270$  pc, MF 83 is one of the three largest SNRs identified in M101 (Matonick & Fesen 1997). It ought to be noted that MF 83 is not a known nonthermal radio source; therefore, strictly speaking, MF 83 should be called a SNR candidate.

The ionized gas in MF 83 is best revealed by the continuum-subtracted  $\text{H}\alpha$  image (Figure 3c). MF 83 apparently consists of an ionized gas shell and a bright  $\text{H II}$  region to the northwest of the shell. The shell is elongated in the NE-SW direction, with an apparent opening at the SW end. The two bright patches of emission along the south rim of the shell have stellar counterparts, indicating that they are  $\text{H II}$  regions. The continuum-subtracted  $[\text{O III}]$  image of MF 83 (Figure 3f) shows a different morphology of the ionized gas. The  $\text{H II}$  regions are much less prominent in the  $[\text{O III}]$  than in the  $\text{H}\alpha$ . The ionized gas shell of MF 83, having higher excitation, is better depicted by the continuum-subtracted  $[\text{O III}]$  image. We have used Kennicutt & Garnett's (1996) spectrophotometry of  $\text{H II}$  regions near NGC 5461 to calibrate the continuum-subtracted  $\text{H}\alpha$  and  $[\text{O III}]$  images and made an  $[\text{O III}]/\text{H}\alpha$  ratio map of MF 83 (Figure 7). It can be seen that the bright  $\text{H II}$  regions have low  $[\text{O III}]/\text{H}\alpha$  ratios, while regions with low surface brightnesses have higher  $[\text{O III}]/\text{H}\alpha$  ratios.

The KPNO 4m green continuum (off- $[\text{O III}]$ ) image in Figure 3e shows four sources, a-d,

in MF 83. Source a is located near the center of the gas shell, while sources b-d are in the H II regions along the south rim of the shell. The *HST* WFPC2 *F547M* image of MF 83 (Figure 4) reveals that all of these four sources are extended and must be OB associations. The discrete sources detected in the WFPC2 *F547M* image are marked in Figure 4; their  $m_{F547M}$  and  $m_V$  magnitudes are tabulated in Table 2. The patch of continuum emission at the shell center (source a in Figure 3e) is resolved into sources 7, 8, 10, 11, and 12 (marked in Figure 4), among which sources 7, 11, and 12 have asymmetric and extended images indicating that they are multiples. The three concentrations of stellar emission along the southern rim of the shell (sources b–d in Figure 3e) are not fully resolved in the WFPC2 *F547M* image, but they (sources 4, 5, and 13) each show irregular, extended spatial structure indicating the existence of multiple stars. Within the compact H II region at the northwest periphery of the shell, stars are also detected, but they are not as highly concentrated or as bright as the stars within the shell and along the south rim of the shell.

The SNR MF 83 presumably corresponds to the shell structure seen in the H $\alpha$  image. The concentration of stars at the shell center probably belongs to an OB association. The three concentrations of stars along the shell rim may represent three distinct OB associations, as their separations are greater than 70 pc and typical sizes of OB associations are  $\leq 70$ –100 pc (Lucke & Hodge 1970; Magnier et al. 1993). There is an additional OB association in the compact H II region at the northwest rim of the shell. The arrangement of these OB associations and H II regions around the shell of MF 83 is reminiscent of the superbubble N11 (Parker et al. 1992; Mac Low et al. 1998) in the Large Magellanic Cloud (LMC). MF 83 is clearly in an environment with star formation.

### 3.2. Physical Properties of the Expanding Shell of MF 83

The echelle observations of MF 83 show that the shell structure shown in the H $\alpha$  and [O III] images is indeed an expanding shell. MF 83 is detected in H $\alpha$ , [N II] $\lambda\lambda 6548, 6584$ , and [S II] $\lambda\lambda 6716, 6731$  lines. The spectral region of H $\alpha$  and [N II] $\lambda 6584$  lines is displayed in the upper panel of Figure 5, and the sky-subtracted H $\alpha$  line is displayed in the lower panel of Figure 5. These line images show clearly a position-velocity ellipse indicating an expanding shell structure. Using the  $2\sigma$  contour level in the sky-subtracted H $\alpha$  line image, we estimate an expansion velocity of  $\sim 50$  km s $^{-1}$  for both the approaching and receding sides of the shell. We will assume that this expanding shell is associated with the supernova remnant in MF 83, and evaluate its mass and kinetic energy.

The shell mass can be derived from the H $\alpha$  luminosity and shell thickness. The H $\alpha$  luminosity of MF 83, computed from the H $\alpha$  flux reported by Matonick & Fesen (1997),



is  $1.7 \times 10^{38}$  ergs  $s^{-1}$ , for a distance of 7.2 Mpc. However, this  $H\alpha$  luminosity includes contributions from the H II regions along the periphery of the expanding shell; these H II regions do not participate in the expansion and hence do not contribute to the shell kinetic energy. To exclude the H II regions, we use the  $H\alpha$  image in conjunction with the [O III] image. As the H II regions have much lower [O III]/ $H\alpha$  ratios than the shell (see Figure 7), we assume that the [O III] flux is dominated by the shell emission, and use the [O III]/ $H\alpha$  ratio in the “clean” part of the shell to convert the [O III] flux to  $H\alpha$  flux. The [O III]/ $H\alpha$  ratio of the entire MF 83 is  $\sim 0.5$ , and the [O III]/ $H\alpha$  of the clean part of the shell is  $\sim 0.7$ . Using these values and the total  $H\alpha$  flux of MF 83, we derive an  $H\alpha$  luminosity of  $1.2 \times 10^{38}$  ergs  $s^{-1}$  for the expanding shell. (Note that this value still over-estimates the shell luminosity, as we have assumed that all [O III] emission originates in the shell.)

The  $H\alpha$  image of MF 83 shows a shell of diameter  $\sim 270$  pc and a fractional shell thickness ( $\Delta R/R$ )  $< 0.5$ . The rms density and mass can be derived from these shell parameters and the  $H\alpha$  luminosity. We have made calculations for  $\Delta R/R = 0.1$  and  $0.5$ , the smallest and largest possible shell thicknesses. We find that the rms density is  $\sim 2.0$ – $1.1$  H  $cm^{-3}$  and the shell mass is  $\sim 1.4$ – $2.5 \times 10^5 M_{\odot}$ . Using this mass and an expansion velocity of  $50$  km  $s^{-1}$ , we find MF 83’s shell kinetic energy to be  $3.5$ – $6.3 \times 10^{51}$  ergs. Finally, if the shell of MF 83 consists of swept-up interstellar medium, the ambient density would be  $0.6$ – $1.0$  H  $cm^{-3}$ . These physical properties of MF 83 shell are summarized in Table 3.

### 3.3. X-ray Emission and Hot Ionized Gas of MF 83

The *ROSAT* HRI observations of MF 83 detected  $118 \pm 20$  counts in the 227-ks exposure. This number of counts (background-subtracted) is in perfect agreement with that reported by Wang, Immler, & Pietsch (1999;  $111 \pm 14$  counts for source H36). Because of this small number of counts, it is difficult to determine accurately whether the X-ray emission is totally unresolved or contains both an unresolved component and a slightly extended component. Figure 6b shows that the position of the X-ray source coincides almost perfectly with the optical boundary of MF 83.

The *ROSAT* PSPC observation of MF 83 detected  $64 \pm 14$  counts (background-subtracted) in the 33.9-ks exposure. This number of counts is 25% higher than that reported by Wang et al. (1999),  $51 \pm 11$  counts, because we used a low background at  $\sim 2'$  NE of MF 83 and our counts may have included more diffuse background within the source aperture. Nevertheless, our number and Wang et al.’s number still agree within the error limits. The observed PSPC count rate of MF 83 is totally consistent with the observed HRI count rate, if we adopt the PSPC to HRI count rate ratio of 3 observed in a wide range of X-ray sources (David et al.

1996). The small number of PSPC counts prohibits meaningful spectral model fits. Compared to other X-ray sources in M101 (Table 5 of Wang et al. 1999), the X-ray emission from MF 83 appears to have a highest hardness ratio HR2 ( $0.79 \pm 0.22$ ), defined to be “(hard1 - hard2)/(hard1 + hard2)” with “hard1” covering channels 52-90 ( $\sim 0.75$  keV) and “hard2” covering channels 91–201 ( $\sim 1.5$  keV). While this hardness ratio is uncertain, it may hint the presence of a hard X-ray component. Future observations with a deeper exposure, a higher angular resolution, and a spectral range covering higher photon energies are needed to resolve the X-ray sources at MF 83.

The PSPC image suggests that the discrete source in MF 83 detected by the HRI is superposed on a diffuse background. As we do not have an effective way to separate the emission of MF 83 from the diffuse background emission, we will use the HRI count rate to represent the emission from MF 83. We assume that all X-ray emission from MF 83 originates from a plasma at  $3 \times 10^6$  K. (This is a reasonable assumption because hot interstellar gas is most frequently observed to be a few  $10^6$  K, and the X-ray emissivity varies very slowly with temperature at this temperature range.) Using a reddening of  $E(B - V) = 0.42$  mag for MF 83 (Matonick & Fesen 1997) and a Galactic gas to dust ratio of  $N_{\text{H}}/E(B - V) = 5.8 \times 10^{21}$  H cm $^{-2}$  mag $^{-1}$  (Bohlin, Savage, & Drake 1978), we obtain a hydrogen column density of  $2.4 \times 10^{21}$  H cm $^{-2}$ . Adopting this hydrogen column density as an approximation for the absorption column density and a  $3 \times 10^6$  K plasma temperature, we find the HRI count rate corresponding to an unabsorbed X-ray flux of  $1.1 \times 10^{-13}$  erg cm $^{-2}$  s $^{-1}$  in the 0.1–2.4 keV band<sup>5</sup>. For a distance of 7.2 Mpc to M101, the X-ray luminosity of the X-ray source in MF 83 is  $6.8 \times 10^{38}$  erg s $^{-1}$ . This luminosity is about five times as high as that reported by Wang (1999),  $1.2 \times 10^{38}$  erg s $^{-1}$ , because Wang et al. assumed a smaller absorption column density and used a smaller counts-to-energy conversion factor.

Our X-ray flux of MF 83 implies an emissivity of  $\sim 2.5 \times 10^{-23}$  erg cm $^3$  s $^{-1}$  for a  $3 \times 10^6$  K plasma with solar abundances. If we assume that the X-ray emitting gas is concentrated in a shell with a certain fractional shell thicknesses ( $\Delta R/R$ ), we may derive the rms density, mass, and thermal energy of the X-ray emitting gas. If  $\Delta R/R = 0.1$ , the rms density, mass, and thermal energy will be  $0.6$  H cm $^{-3}$ ,  $4 \times 10^4 M_{\odot}$ , and  $2.9 \times 10^{52}$  ergs, respectively; if  $\Delta R/R = 0.5$ , these figures will be  $0.3$  H cm $^{-3}$ ,  $7 \times 10^4 M_{\odot}$ , and  $5.2 \times 10^{52}$  ergs, respectively.

---

<sup>5</sup>calculated by using W3PIMMS tool at <http://heasarc.gsfc.nasa.gov/Tools/w3pimms.html>

## 4. Discussion

The SNR MF 83 in M101 is intriguing because it has been suggested to be a hypernova remnant and it may need an explosion energy comparable to those associated with GRBs (Wang 1999). Our new observations allow us to examine critically the physical nature of MF 83. We will first compare MF 83 to known, common astronomical objects and assess the likelihood that MF 83 has a similar nature. We will then consider the possibility of the existence of an energetic SNR and evaluate its energetics.

### 4.1. MF 83 as a Star Formation Region

MF 83 consists of a  $\sim 270$  pc ionized gas shell, three H II regions along the south rim and another H II region outside the northwest rim of the shell. This arrangement is commonly seen in star formation regions. These H II regions individually have an H $\alpha$  luminosity of  $\sim 2 \times 10^{37}$  ergs s $^{-1}$ . This H $\alpha$  luminosity requires an ionizing flux of  $\sim 2 \times 10^{49}$  ionizing photons s $^{-1}$ , which can be easily supplied by an O6 star or several later-type O stars. The presence of late-type O stars, or a lack of early-type O stars, is also supported by the low [O III]/H $\alpha$  ratios of the H II regions.

The stellar continuum sources detected in the WFPC2 *F547M* images have absolute visual magnitudes  $M_V$  in the range of  $-6$  to  $-8$  mag (Table 2). While the faintest sources might be single early-type supergiants, the brighter sources and especially the sources showing asymmetric or extended images are composites, e.g., sources 4, 5, 12, and 13 in Table 2 and Figure 4. The composite sources embedded in H II regions (sources 4, 5, and 13) and the composite source at the shell center (source 12) are most likely OB associations.

The H II regions and OB associations in MF 83 are only about twice as powerful as the Orion Nebula, and are comparable to the less impressive OB/H II regions in the LMC. MF 83 is a star formation region, but by no means a starburst region.

### 4.2. The Supernova Remnant Candidate in MF 83

The existence of a SNR in MF 83 is suggested by the high [S II]/H $\alpha$  ratio, 0.76 (Mattonick & Fesen 1997), and bright X-ray emission,  $1.2 \times 10^{38}$  ergs s $^{-1}$  (Wang 1999). These two properties, unfortunately, cannot unambiguously ensure the existence of a SNR for the following reasons. First, the [S II]/H $\alpha$  ratio is high for both low-velocity shocks (shock velocity  $\leq 50$  km s $^{-1}$ ) and high-velocity shocks (shock velocity  $\geq 100$  km s $^{-1}$ ) (Shull & McKee

1979). While SNRs with large shock velocities show high  $[\text{S II}]/\text{H}\alpha$  ratios, superbubbles with expansion velocities approaching  $50 \text{ km s}^{-1}$  also show high  $[\text{S II}]/\text{H}\alpha$  ratios, for example, the superbubbles N185 and N186E in the LMC have  $[\text{S II}]/\text{H}\alpha$  ratios of 0.64 and  $\sim 1$ , respectively (Lasker 1977). Second, the X-ray source in MF 83 is not resolved by the *ROSAT* HRI or PSPC. Moreover, the PSPC spectral hardness ratio of MF 83 suggests the existence of a hard component, which is frequently associated with X-ray binaries, and the X-ray luminosity of MF 83 is within the range of luminosities seen in X-ray binaries in M101 (Wang et al. 1999). Therefore, until the X-ray source is shown to be spatially extended or the radio spectral index is observed to be nonthermal, the existence of a SNR in MF 83 is not confirmed.

### 4.3. The Large Expanding Shell as an X-ray-bright Superbubble

The large shell in MF 83 was initially identified as the SNR (Matonick & Fesen 1997). As we have illustrated in §4.1, this large shell is centered on groups of stars that are likely to be OB associations. The large shell size and the central stellar content suggest that this shell is a superbubble. It is then interesting to compare the physical properties of this large shell in MF 83 to those of known superbubbles in the LMC, which have been extensively studied. Most LMC superbubbles with sizes greater than 100 pc have expansion velocities well below  $50 \text{ km s}^{-1}$  (Georgelin et al. 1983; Rosado 1986), with N185 being the only exception (diameter  $\sim 105 \text{ pc}$ , expansion velocity =  $70 \pm 10 \text{ km s}^{-1}$ , Rosado et al. 1982). The  $50 \text{ km s}^{-1}$  expansion velocity and 270-pc diameter of MF 83 thus make it unusual: it is unusually large for its expansion velocity, or it expands unusually fast for its size.

The expansion velocity of the MF 83 shell implies a shock velocity of  $\sim 67 \text{ km s}^{-1}$ . The post-shock region should have a high  $[\text{O III}]/\text{H}\alpha$  ratio, but not larger than 1.0 (Shull & McKee 1979; Hartigan, Raymond, & Hartmann 1987). This is consistent with the observed high  $[\text{O III}]/\text{H}\alpha$  ratio in the shell,  $\sim 0.7$ . This shock velocity may also be responsible for the high  $[\text{S II}]/\text{H}\alpha$  ratio observed in the MF 83 shell, but is not high enough to produce X-ray emission in the post-shock region. The high  $[\text{S II}]/\text{H}\alpha$  ratio and bright X-ray emission must not originate from the same shocks. If the X-ray emission from MF 83 is indeed diffuse and originates in the shell interior, the MF 83 shell would be similar to the X-ray-bright superbubbles in the LMC, which have been suggested to be powered by interior SNRs near the shell walls (Chu & Mac Low 1990; Wang & Helfand 1991). Many X-ray-bright superbubbles in the LMC are known to expand faster than expected and have high  $[\text{S II}]/\text{H}\alpha$  ratio (Oey 1996). It is possible that the large shell in MF 83 is an X-ray-bright superbubble.

As an X-ray-bright superbubble, the MF 83 shell is unusually large for its expansion velocity and is exceptionally luminous in X-rays. Compared to the X-ray-brightest super-

bubble in the LMC, N44 (Chu et al. 1993), the MF 83 superbubble is  $\sim 500$  times more luminous. The internal thermal energy implied by the X-ray emission is a few  $\times 10^{52}$  ergs. It is conceivable that the high thermal pressure, resultant from this large thermal energy, drives the fast expansion of the superbubble. However, this amount of thermal energy is more than an order of magnitude higher than the canonical explosion energy of a supernova. If the large shell in MF 83 is an X-ray-bright superbubble, it requires either a “hypernova” or 10–100 normal supernovae within the past  $\sim 1 \times 10^6$  years, the cooling time scale for a hot gas with a temperature of  $3 \times 10^6$  K and density of  $0.5 \text{ H cm}^{-3}$ .

#### 4.4. The Large Expanding Shell as a Hypernova Remnant

Finally, we consider the possibility that the large shell of MF 83 is formed by one single energetic explosion. Our analyses in §3.2 and §3.3 show a kinetic energy of a few  $\times 10^{51}$  ergs in the ionized gas shell, and an internal thermal energy of a few  $\times 10^{52}$  ergs in the shell interior. A similar disparity between the ionized shell kinetic energy and internal thermal energy has been seen in the X-ray-bright superbubble N44, but it is found that the ionized shell of N44 is enveloped by a co-expanding, more massive, neutral H I shell (Kim et al. 1998). It is possible that the MF 83 shell also has a neutral shell carrying more mass and kinetic energy than the ionized shell. The kinetic energy in the ionized gas shell is thus a lower limit on the shell kinetic energy, and cannot be used to determine the explosion energy.

If the MF 83 shell is formed by one single explosion, the explosion energy must be greater than the observed internal thermal energy, and may approach  $10^{53}$  ergs, which is about two orders of magnitude higher than the canonical explosion energy for a normal supernova (Jones et al. 1998). This large energy requirement would qualify MF 83 as a “hypernova remnant.” However, to prove that MF 83 is indeed a hypernova remnant, it is necessary to demonstrate convincingly that a single explosion formed the MF 83 shell. The existence of OB associations within MF 83 provides circumstantial evidence that multiple explosions produced the shell, but this neither demonstrates or rules out that a dominant powerful explosion occurred.

## 5. Summary and Conclusions

The SNR candidate MF 83 in M101 has been suggested to be a hypernova remnant that requires an explosion energy about two orders of magnitude higher than those of normal supernovae, based mainly on the high X-ray luminosity of MF 83 and the assumption that

all X-ray emission originates from shock-heated gas in the remnant.

We have analyzed high-quality ground-based and *HST* images of MF 83, and found that MF 83 is a star formation region. The  $H\alpha$  images show that MF 83 consists of four H II regions and a large ionized shell. The stellar continuum images show groups of stars in the H II regions and within the shell; these groups of stars are most likely OB associations.

The stellar content and physical properties of the large shell in MF 83 suggest that it is a superbubble. If the X-ray emission is indeed diffuse, this shell will be an X-ray-bright superbubble whose interior has been heated by recent supernovae. The thermal energy derived from the X-ray data is a few  $\times 10^{52}$  ergs, which requires either a “hypernova” or 10–100 normal supernovae in the past  $10^6$  years. If it can be proved that the shell of MF 83 is produced by one single explosion, then a “hypernova” may be in order.

Future X-ray observations with high angular resolution is needed to resolve the X-ray source in MF 83. Only after excluding point sources in MF 83 can we determine the true amount of diffuse X-ray emission, re-evaluate the energy budgets, and assess the “hypernova remnant” nature of MF 83.

This research is partially supported by the grant STScI GO-6829.01-95A, and uses observations with the NASA/ESA *Hubble Space Telescope*, obtained at the Space Telescope Science Institute, which is operated by the AURA, Inc., under NASA contract NAS5-26555. This paper also uses data obtained (in part) with the 2.4 m Hiltner Telescope of the Michigan-Dartmouth-MIT Observatory. SPL thanks the support by the Laboratory for Astronomical Imaging through NSF grants AST 96-13999 and AST 98-20641. EKG gratefully acknowledges support by NASA through grant HF-01108.01-98A from the Space Telescope Science Institute.

## REFERENCES

- Biretta, J. A., et al. 1996, WFPC2 Instrument Handbook, Version 4.0 (Baltimore: STScI)
- Bohlin, R. C., Savage, B. D., & Drake, J. F. 1978, *ApJ*, 224, 132
- Chu, Y.-H., Chen, C.-H. R., & Lai, S.-P. 2000, *HST* May Symposium 1999, “The Largest Explosions Since the Big Bang: Supernovae and Gamma-Ray Bursts”, (astro-ph/9909091), in press
- Chu, Y. -H., & Kennicutt, R. C., Jr. 1986, *ApJ*, 311, 85
- Chu, Y.-H., & Mac Low, M.-M. 1990, *ApJ*, 365, 510
- Chu, Y.-H., Mac Low, M.-M., García-Segura, G., Wakker, B., & Kennicutt, R. C. Jr. 1993, *ApJ*, 414, 213
- David, L. P., Harnden, F. R., Jr., Kearns, K. E., & Zombeck, M. V. 1996, The *ROSAT* High Resolution Imager (HRI) Calibration Report, published by U.S. *ROSAT* Science Data Center/SAO (updated 1997)
- Feldmeier, J. J., Ciardullo, R., & Jacoby, G. H. 1997, *ApJ*, 479, 231
- Georgelin, Y. M., Georgelin, Y. P., Laval, A., Monnet, G., & Rosado, M. 1983, *A&AS*, 54, 459
- Harris, F. J. 1978, *Proceedings of the IEEE*, 66, 51
- Hartigan, P., Raymond, J., & Hartmann, L. 1987, *ApJ*, 316, 323
- Holtzman, J. A., et al. 1995a, *PASP*, 107, 156
- Holtzman, J. A., Burrows, C. J., Casertano, S., Hester, J. J., Trauger, J. T., Watson, A. M., & Worthey, G. 1995b, *PASP*, 107, 1065
- HST* Data Handbook 1998 Version 3.1, Vol. I, ed. R. Shaw
- Jones, T. W., et al. 1998, *PASP*, 110, 125
- Kennicutt, R. C., Jr., & Garnett, D. R. 1996, *ApJ*, 456, 504
- Kim, S., Chu, Y.-H., Staveley-Smith, L., & Smith, R. C. 1998, *ApJ*, 503, 729
- Lasker, B. M. 1977, *ApJ*, 212, 390
- Lucke, P. B., & Hodge, P. W. 1970, *AJ*, 75, 171
- Mac Low, M. -M., Chang, T. H., Chu, Y. -H., Points, S. D., Smith, R. C., & Wakker, B. P. 1998, *ApJ*, 493, 260
- Magnier, E. A., et al. 1993, *A&A*, 278, 36
- Matonick, D. M., & Fesen, R. A. 1997, *ApJS*, 112, 49

- Oey, M. S. 1996, *ApJ*, 467, 666
- Paczynski, B. 1998, *ApJ*, 494, L45
- Paczynski, B. 2000, *HST* May Symposium 1999, “The Largest Explosions Since the Big Bang: Supernovae and Gamma-Ray Bursts”, (astro-ph/9909048), in press
- Parker, J. W. , Garmany, C. D., Massey, P., & Walborn, N. R. 1992, *AJ*, 103, 1205
- Rosado, M. 1986, *A&A*, 160, 211
- Rosado, M., Georgelin, Y. M., Georgelin, Y. P., Laval, A., & Monnet, G. 1982, *A&A*, 115, 61
- ROSAT* Mission Description. 1991, NASA pub. NRA 91-OSSA-3, App. F (updated 1995)
- Shafter, A. W., Ciardullo, R., & Pritchett, C. J. 2000, *ApJ*, 530, 193
- Shull, J. M., & McKee, C. F. 1979, *ApJ*, 227, 131
- Skillman, E. D. 1985, *ApJ*, 290, 449
- Stetson, P. B., et al. 1998, *ApJ*, 508, 491
- Wang, Q. D. 1999, *ApJ*, 517, L27
- Wang, Q., & Helfand, D. J. 1991, *ApJ*, 373, 497
- Wang, Q. D., Immler, S., & Pietsch, W. 1999, *ApJ*, 523, 121
- Whitmore, B., & Heyer, I. 1995, Instrument Science Report WFPC2 95-04 (also available at the WFPC2 website [http://www.stsci.edu/instruments/wfpc2/wfpc2\\_doc.html#Phot](http://www.stsci.edu/instruments/wfpc2/wfpc2_doc.html#Phot))



Table 1: Journal of KPNO 4m Echelle Observations

Date of observation	Slit orientation	Slit width	Exposure time	Instrumental FWHM
1999 March 4	NS	2"0	1×1800 s	19.0±1.6 km s <sup>-1</sup>
1999 June 30	EW	1"5	4×1800 s	14.9±0.6 km s <sup>-1</sup>
1999 July 1	NS	2"0	3×1800 s	18.3±0.5 km s <sup>-1</sup>

Table 2: Photometry of Bright Stellar Sources in MF83

ID	R.A. (J2000)	Decl. (J2000)	$m_{F547M}^a$ mag	$M_V^b$ mag
1	14 3 35.67	54 19 26.92	24.6	-6.1
2	14 3 35.76	54 19 29.27	24.3	-6.3
3	14 3 35.77	54 19 18.85	24.9	-5.8
4	14 3 35.80	54 19 20.90	22.6	-8.1
5	14 3 35.98	54 19 19.88	22.9	-7.8
6	14 3 36.05	54 19 20.76	24.7	-6.0
7	14 3 36.05	54 19 22.78	23.4	-7.3
8	14 3 36.05	54 19 24.34	24.5	-6.1
9	14 3 36.09	54 19 19.46	24.7	-6.0
10	14 3 36.15	54 19 25.71	24.8	-5.9
11	14 3 36.16	54 19 24.35	24.0	-6.7
12	14 3 36.17	54 19 23.41	22.7	-7.9
13	14 3 36.35	54 19 20.46	23.2	-7.4
14	14 3 36.66	54 19 23.15	23.4	-7.2
15	14 3 36.73	54 19 22.25	24.3	-6.4

<sup>a</sup>Apparent magnitude in the WFPC2  $F547M$  bandpass. The photometric error is  $\sim 0.2$  mag.

<sup>b</sup>Assuming an extinction of  $A_V = 1.3$  mag (Matonick & Fesen 1997) and a distance of 7.2 Mpc (Stetson et al. 1998).

Table 3: Physical Properties of MF 83

Shell thickness ( $\Delta R/R$ )	0.1	0.5
Electron density ( $\text{cm}^{-3}$ )	2.0	1.1
Mass of the shell ( $10^5 M_{\odot}$ )	1.4	2.5
Ambient density ( $\text{cm}^{-3}$ )	0.6	1.0
Kinetic energy ( $10^{51}$ ergs)	3.5	6.3

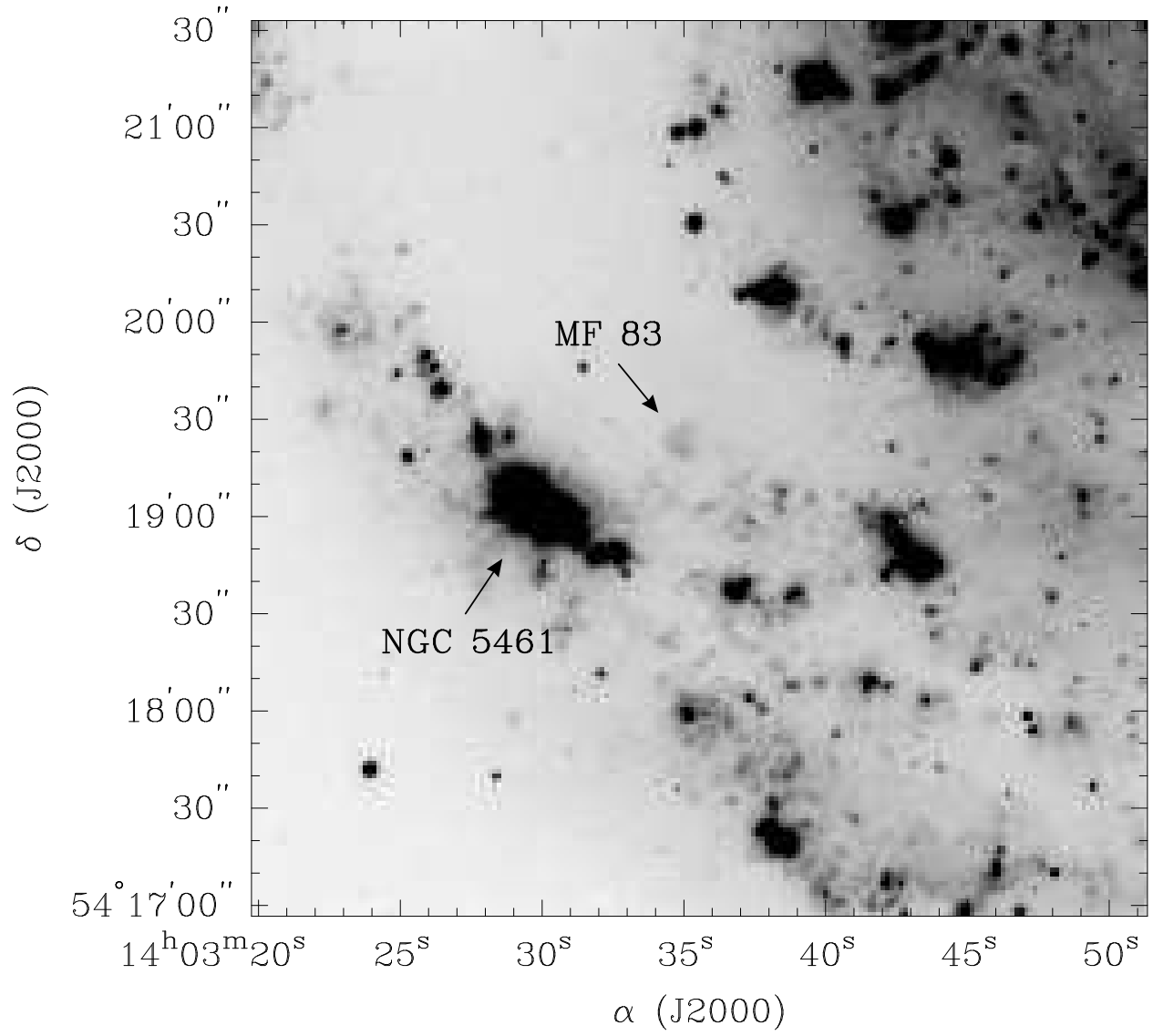


Fig. 1.— MDM 2.4m H $\alpha$  image of MF83 and an eastern portion of M101.

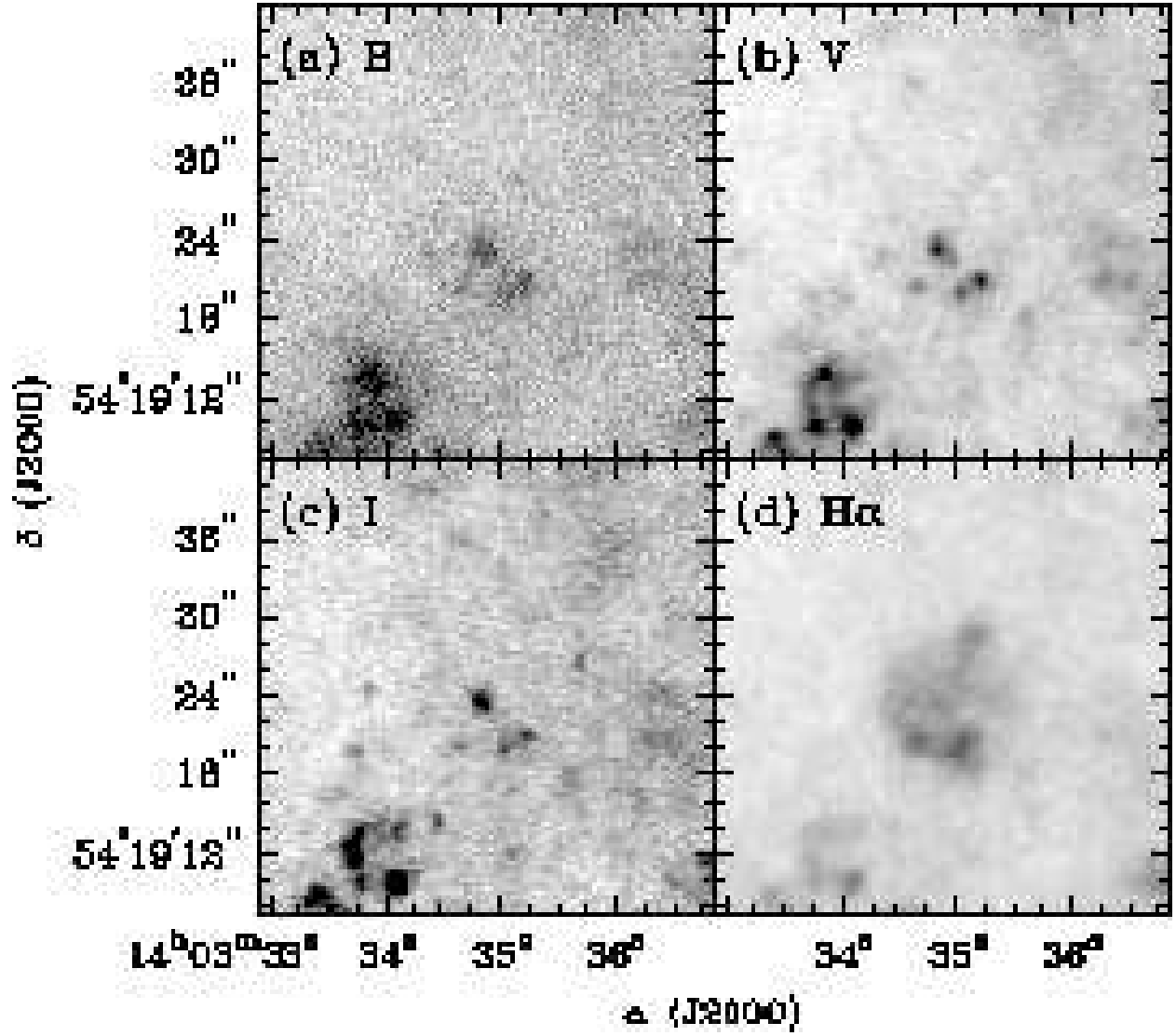


Fig. 2.— MDM 2.4m images of MF 83 in the (a) *B*, (b) *V*, (c) *I* bands and the (d)  $H\alpha$  line. The field of view of each plot is  $35'' \times 35''$ .

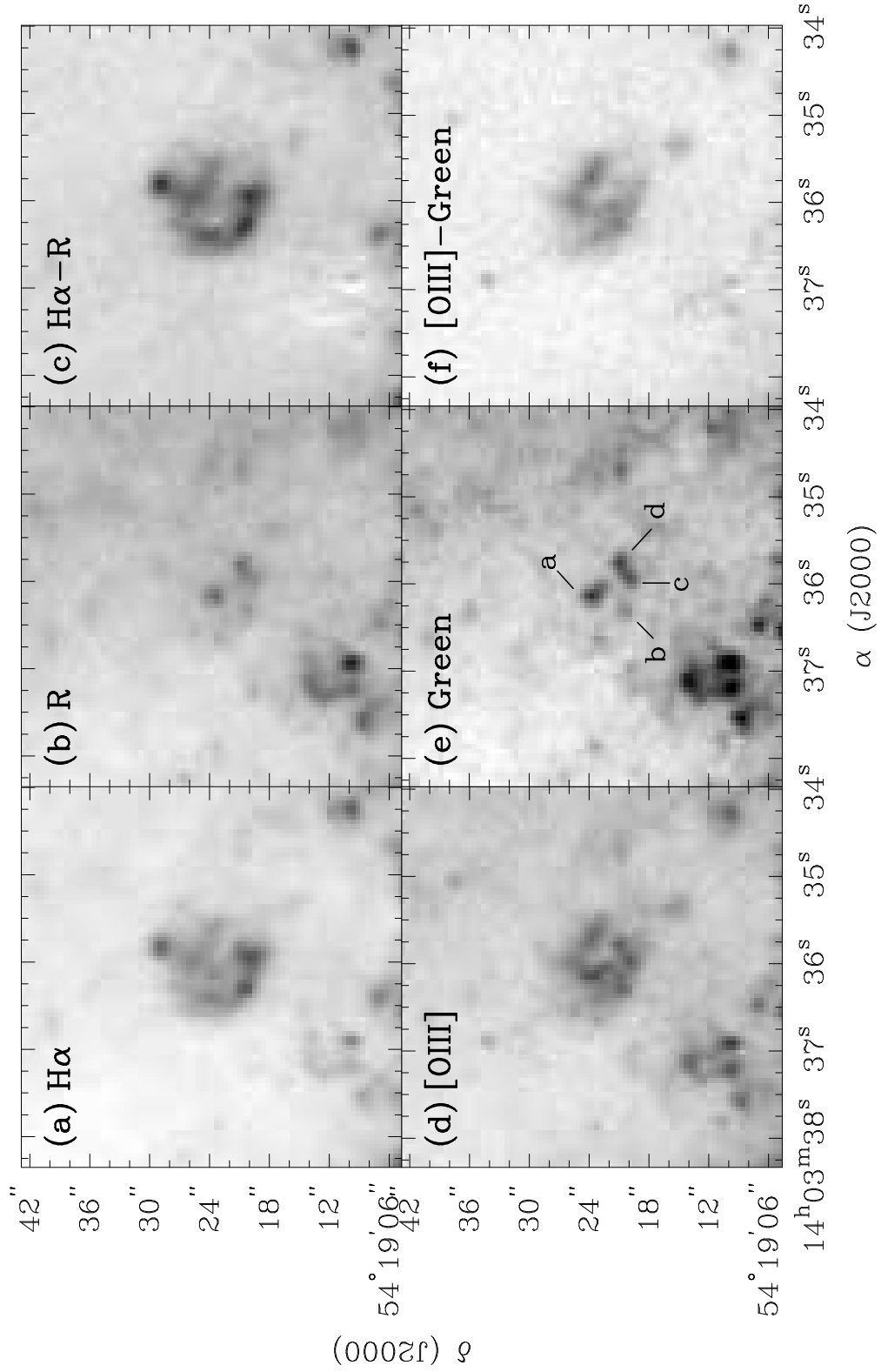


Fig. 3.— KPNO 4m images of MF 83 in (a)  $H\alpha$ , (b) R band, (c) continuum-subtracted  $H\alpha$ , (d)  $[OIII]$ , (e) green continuum, and (f) continuum-subtracted  $[OIII]$ . Four concentrations of stars, a–d, are marked in (e).

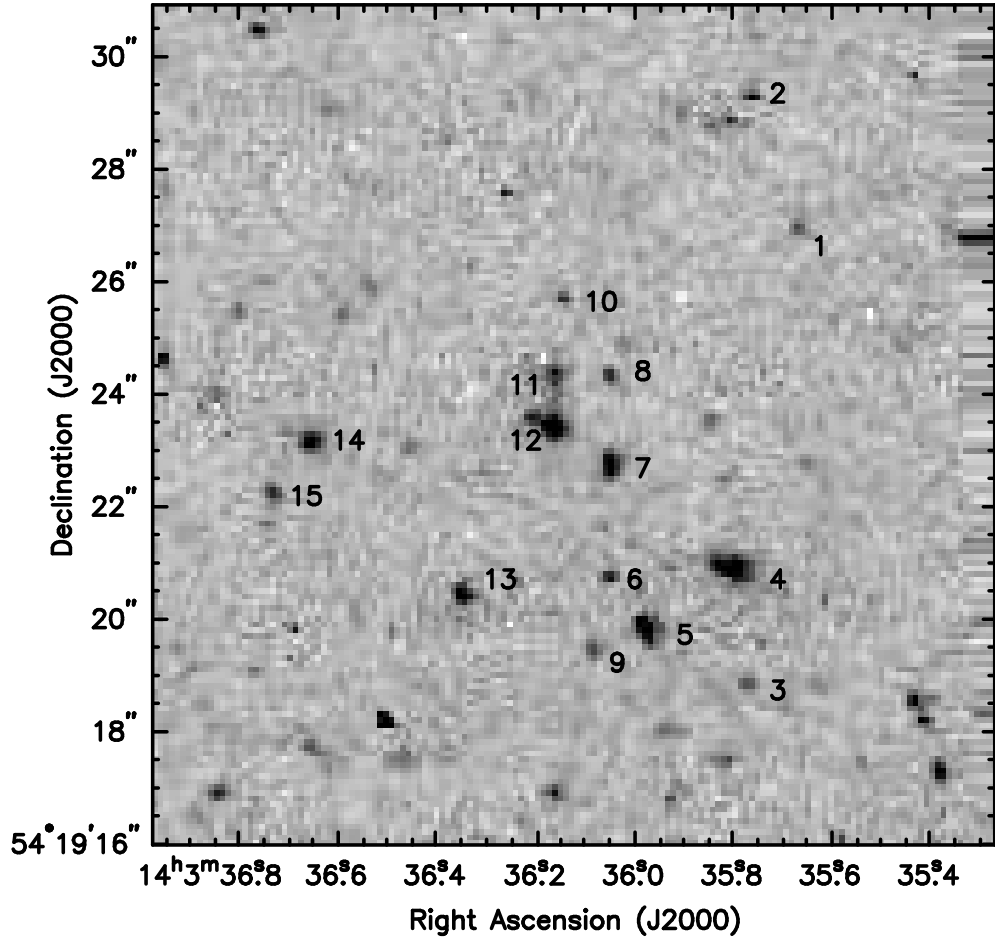


Fig. 4.— *HST* WFPC2 image of MF 83 in the *F547M* band. The photometry of the sources marked is given in Table 2.

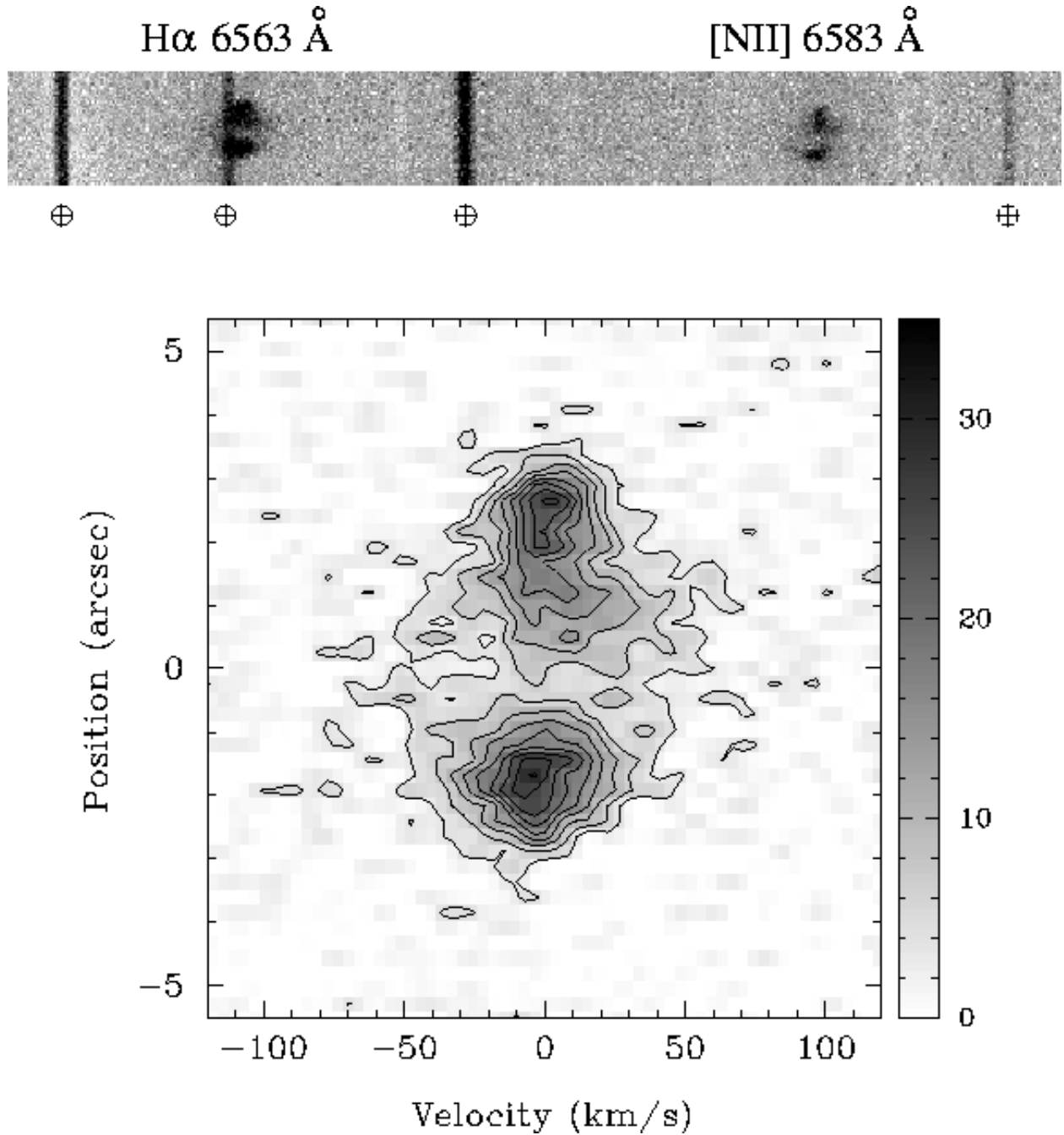


Fig. 5.— Top: KPNO 4m echelle image of the H $\alpha$  and [NII] lines for a N-S slit position centered on MF 83. The telluric lines marked by  $\oplus$  are OH 6553.6 Å, H $\alpha$  6562.8 Å, OH 6568.8 Å, and OH 6577.2/6577.4 Å. Bottom: The sky-subtracted H $\alpha$  line from the above echellogram, Hanning smoothed over five pixels along the velocity axis. The  $1\sigma$  noise level is 1.6 counts pixel $^{-1}$ . The contours are at 2, 4, 6, 8, 10, 12, 14, and 16  $\sigma$  levels.



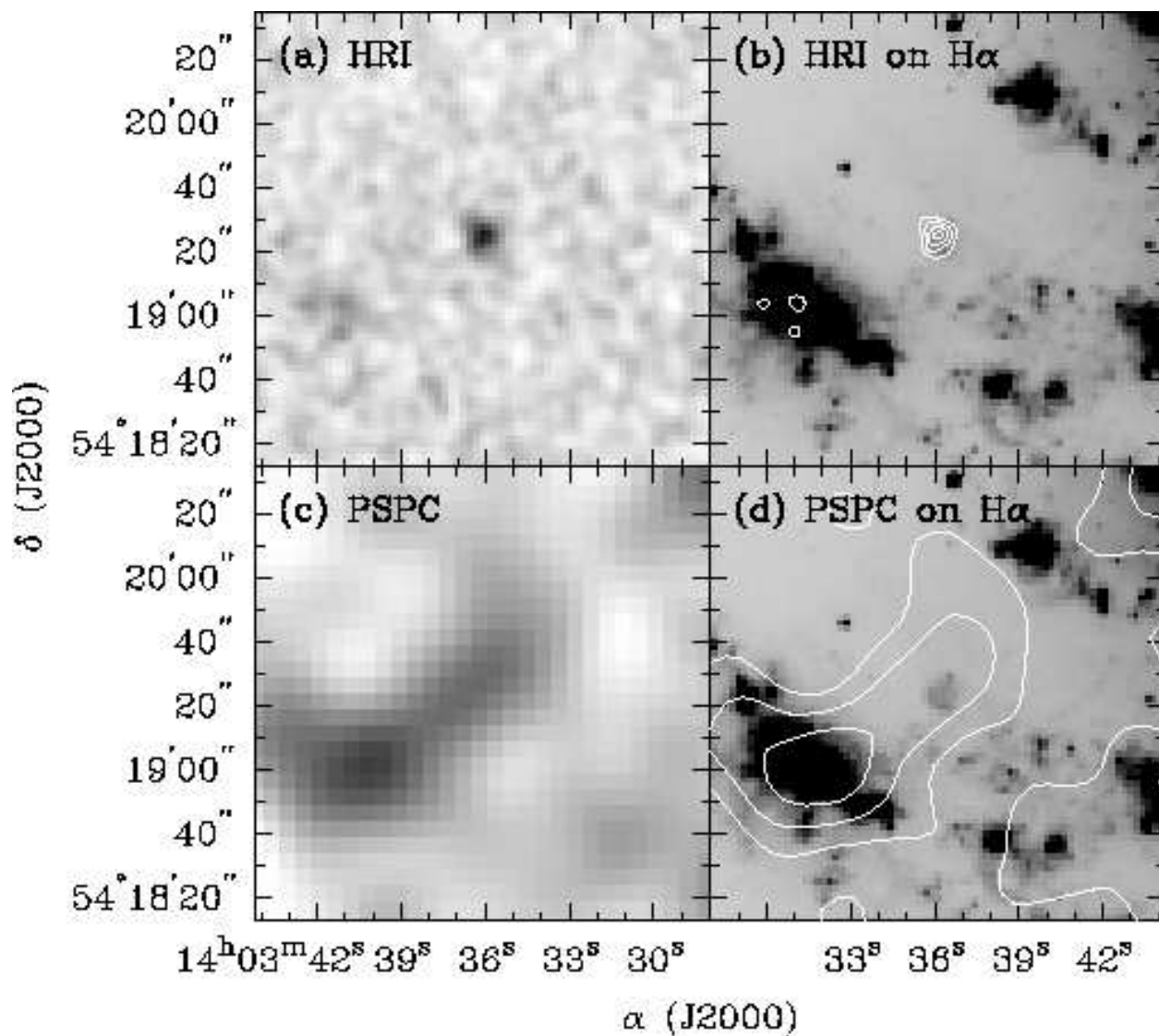


Fig. 6.— *ROSAT* X-ray images of MF 83. (a) HRI image in greyscale. This HRI image has been smoothed with a Gaussian of  $\sigma = 1''$ . (b) HRI contours over the KPNO 4m  $\text{H}\alpha$  image. The contour levels are 45, 60, 75, 90% of the peak. (c) PSPC image in greyscale. This PSPC image has been smoothed with a Gaussian of  $\sigma = 10''$ . (d) PSPC contours over the KPNO 4m  $\text{H}\alpha$  image. The contour levels are 1.2, 1.5, 1.8 counts  $\text{pixel}^{-1}$ .

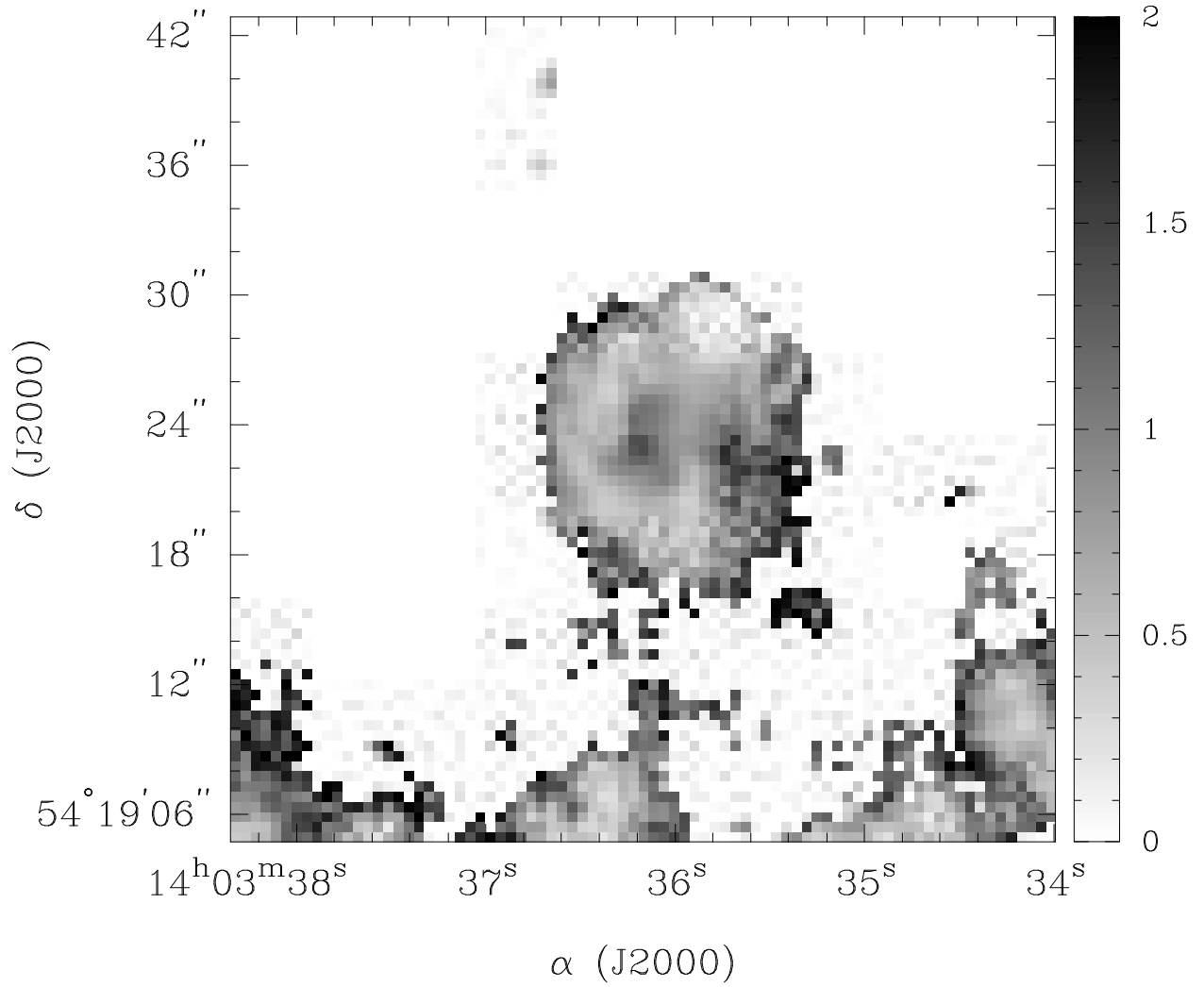


Fig. 7.— [O III]/H $\alpha$  ratio map of MF 83. The grey scale bar on the right shows the [O III]/H $\alpha$  range of 0–2.0.